

Multi-component secluded WIMP dark matter and Dirac neutrino masses with an extra Abelian gauge symmetry

Kimy Agudelo,^{*} Diego Restrepo,[†] Andrés Rivera,[‡] and David Suarez[§]

*Instituto de Física, Universidad de Antioquia,
Calle 70 No. 52-21, Medellín, Colombia.*

(Dated: December 20, 2024)

Abstract

Scenarios for secluded WIMP dark matter models have been extensively studied in simplified versions. This paper shows a complete UV realization of a secluded WIMP dark matter model with an extra Abelian gauge symmetry that includes two-component dark matter candidates, where the dark matter conversion process plays a significant role in determining the relic density in the Universe. The model contains two new unstable mediators: a dark Higgs and a dark photon. It generates Dirac neutrino masses and can be tested in future direct detection experiments of dark matter. The model is also compatible with cosmological and theoretical constraints, including the branching ratio of Standard model particles into invisible, Big Bang nucleosynthesis restrictions, and the number of relativistic degrees of freedom in the early Universe, even without kinetic mixing.

Keywords: Dark matter, Neutrino masses, secluded WIMP.

* kimy.agudelo@udea.edu.co

† restrepo@udea.edu.co

‡ afelipe.rivera@udea.edu.co

§ david.suarezr@udea.edu.co

I. INTRODUCTION

Cosmology requires a heavy neutral stable particle to be a viable dark matter (DM) candidate. Neutrino oscillation data need a plausible mechanism that generates neutrino masses, but the standard model (SM) lacks both. Thus, an extension of SM is required.

A popular paradigm of DM is the secluded WIMP [1], where the processes leading to the relic abundance of DM occur in the dark sector. DM candidates mainly annihilate into lighter mediators that can decay into SM states, particularly into neutrinos. Consequently, the right value of the relic abundance of DM is obtained. An extra Abelian dark gauge symmetry with the corresponding dark photon provides a suitable scenario for secluded WIMP DM [2], where the spontaneous symmetry breaking of the Abelian gauge symmetry leaves the remaining discrete symmetries that allow for two-component DM. One suitable DM candidate comes in just one flavor. Two different flavor eigenstates mix in another dark sector to form mass eigenstates. The lightest of them is a suitable DM candidate. The two dark matter candidates interact via the dark photon and the dark Higgs when the masses of scalar fields that generate neutrino masses are too heavy.

On the other hand, the non-observation of neutrinoless double beta decay opens the possibility of neutrinos as Dirac fermions. If they are Dirac fermions, neutrinos, and antineutrinos differ, and the total lepton number is conserved. The extra Abelian gauge symmetry guarantees lepton number conservation and is responsible for the stability of the DM candidates in the dark sectors. In this scenario, we generate Dirac neutrino masses at one-loop via a scotogenic realization of the effective operator for Dirac neutrino masses in the SM [3].

We explain the generalities of the secluded models in Sec. II. We describe our model in Sec. III. In Sec. IV, we explain the DM considerations within our model. In Sec. V, we present the phenomenology of the model, the DM analysis, the numerical results, the status, and the prospects for DM searches. We conclude in Sec. VI.

II. SECLUDED GAUGE MODELS WITH CHIRAL FERMIONS

In a fundamental theory, the elementary fermions are expected to be massless chiral fields. Their masses emerge through Yukawa terms, which are allowed by the respective charges via some scalar that triggers spontaneous symmetry breaking (SSB). For a set of such charges associated with the N chiral fields under a $U(1)$ gauge symmetry

$$\mathbf{Z} = [Z_1, Z_2, \dots, Z_N],$$

at least the linear anomaly (with one $U(1)$ gauge boson and two gravitons on the external lines) and the cubic anomaly (with three $U(1)$ gauge bosons on the external lines) must be cancelled [4–8],

$$\sum_{i=1}^N Z_i = 0, \quad \sum_{i=1}^N Z_i^3 = 0. \quad (1)$$

In fact, in the standard model (SM), for each chiral generation, there exists a solution to eq. (1) for the gauge Abelian symmetry $U(1)_Y$. Expressed in terms of 15 non-opposite-sign integers, the solution ¹

$$\mathbf{Y} = [1, 1, 1, 1, 1, 1, -4, -4, -4, 2, 2, 2, -3, -3, 6],$$

corresponds to the hypercharges of 15 left-handed Weyl massless fermions. The SSB is triggered by a Higgs, H , of hypercharge 3. This leads to Yukawa interactions through the Dirac pairs

$$u_\alpha = (1, -4), (1, -4), (1, -4), \quad d_\alpha = (1, 2), (1, 2), (1, 2), \quad e = (-3, 6).$$

Consequently, 14 of the chiral fermions acquire Dirac masses after the SSB. Each set of quark Dirac fermions is degenerated due to the additional color symmetry. A left-handed Weyl fermion, ν_L , with hypercharge -3 , remains massless, while the remnant Z_3 symmetry guarantees the stability of the lightest quark.

Similarly, the dark matter of the Universe would be part of a dark sector that contains a self-consistent set of chiral fermions that satisfy eq. (1) under the charges of a secluded

¹ There is factor 1/6 between this convention and the more common one.

gauge Abelian symmetry, $U(1)_D$, where all the SM particles are neutral. Following the SSB via a dark Higgs mechanism, the lightest massive fermion could be a viable candidate for fermionic dark matter. This work explores the general phenomenological features of a secluded dark sector with chiral fermions and inert scalars where the dark photon and the dark Higgs act as mediators [9]. Similarly to the SM, the charges of the chiral fermions in the solution should not allow a mass term larger than the scale of the SSB. To relax the constraints from the kinetic mixing [10], those models [11] allow an additional annihilation channel for the fermionic dark matter candidate into SM Dirac neutrinos [2]. If the right-handed components of these neutrinos couple directly to the dark photon, these Weyl fermions can be identified with the remaining chiral massless fermions in the solution after the SSB in the dark sector [2, 12, 13].²

Models with a tree-level contribution to the Dirac neutrino masses are automatically forbidden. However, the effective Dirac neutrino mass operator can be allowed through the dark Higgs, S [3]

$$\mathcal{L} = w_{\alpha i} (\nu_{R\alpha})^\dagger L_i H S^\delta, \quad \delta = 1, 2. \quad (2)$$

Notice that we need at least two right-handed neutrinos with secluded degenerated charges to explain the neutrino oscillation data [3]. Approximately one thousand solutions to eq. (1) were found up to 12 chiral fields and charges of up to 20 in absolute value. Each solution features at least two repeated integers to be assigned as the charges of the right-handed neutrinos. All other chiral fermions in the solution acquire masses after SSB via interactions with the dark Higgs. This results in a dark sector with multi-component dark matter candidates, with at least two-component dark matter candidates in the simpler scenarios.

To ensure the two-mediator scenario, we assume that the effective Dirac neutrino operator is realized only at the radiative level, mediated by a decoupled scalar inert sector that does not develop vacuum expectation values. Here, we focus on a two-component DM model. To maintain a simple inert scalar structure where the neutrino Dirac masses are generated at one-loop [12, 13]. The simplest solution in this case corresponds to the one

² In another class of secluded solutions, proposed to explain the reactor anti-neutrino anomaly [14], these fermions may also be interpreted as sterile neutrinos [4, 6, 15, 16].

with 9 chiral fermions

$$\mathbf{D} = [9, 9, 9, (1, -10), (1, -10), (-4, -5)], \quad (3)$$

and a dark Higgs with a charge of 9. Notice that one of the right-handed neutrinos of charge 9 remains massless. In this scenario, the first dark matter candidate is the lightest state of two Dirac fermions associated with the pairs $(1, -10)$ and the other DM candidate is the Dirac fermion associated with the pair $(-4, -5)$ [12, 13].

The phenomenological analysis presented in this paper is valid for all the thousand models found in the previous work [3], provided that the extra chiral fermions and inert scalars remain sufficiently decoupled from our two-mediator and two-component dark matter scenario. This applies from the simpler case with only six chiral fermions: $[5, 5, (1, -6), (-2, -3)]$, and a dark Higgs with charge 5, with two-component dark matter candidates but with a more complicated inert scalar sector [13]. An interesting case has 12 chiral fermions and a minimal inert scalar sector: $[-9, -9, -9, (3), (3), (3), (1, 5), (1, 5), (-7, 13)]$, with a dark Higgs of charge 6. In that case, all three right-handed neutrinos of charge -9 generate masses and mixings of three Dirac neutrinos through a Dirac scotogenic mechanism with Majorana mediators [17] of charge 3, which are part of the three-component and multiflavor dark matter candidates in the model.

III. DESCRIPTION OF THE MODEL

Tab. I shows new fields added to our model. The first five fields in the table correspond to an anomaly-free set of left-handed chiral fermions, singlets under the symmetry group of SM, including the right-handed neutrinos, $\nu_{R\alpha}$. Regarding the scalar fields that acquire VEV in the model, we have H , the SM Higgs doublet; S is an SM singlet scalar that spontaneously breaks the extra Abelian gauge symmetry. The last two fields in the table compose the inert scalar sector required for the scotogenic realization of chiral models, where η is a $SU(2)_L$ scalar doublet, Φ is an SM-singlet scalar. This table also shows the charges under the $U(1)_D$ symmetry. Notice that we have a dark photon corresponding to the dark symmetry. This model is a benchmark scenario for chiral dark matter with scotogenic Dirac neutrino masses with two-mediator and two-component fermionic dark matter where one

Field	Generations	$SU(2)_L$	$U(1)_Y$	$U(1)_D$
$(\nu_{R\alpha})^\dagger$	3	1	0	-9
χ_L	1	1	0	4
$(\chi_R)^\dagger$	1	1	0	5
ψ_{Li}	2	1	0	10
$(\psi_{Ri})^\dagger$	2	1	0	-1
H	1	2	-1/2	0
S	1	1	0	-9
η	1	2	-1/2	-1
Φ	1	1	0	-1

Table I. Fermion and scalar content with its quantum numbers.

Dirac fermion has just one generation and the second dark matter candidate is the lightest mass eigenstate of mixing with two flavors.

The most general Lagrangian, invariant under the SM group and the new $U(1)_D$ symmetry is given by (in two-component notation):

$$-\mathcal{L} \supset y_c \chi_R^\dagger \chi_L S + (y_x)^{ij} \psi_{Ri}^\dagger \psi_{Lj} S + (y_{nR})^{\alpha i} \nu_{R\alpha}^\dagger \psi_{Li} \Phi + (y_{nL})^{i\alpha} \psi_{Ri}^\dagger L_\alpha \cdot \tilde{\eta} + \text{h.c.}, \quad (4)$$

where (\cdot) is the $SU(2)_L$ dot product, $\tilde{\eta} = (\eta^+, -\eta^0)^T$, $\alpha, = 1, 2, 3$, $i = 1, 2$. and the Yukawa couplings y are assumed real parameters. Also, the Lagrangian contains the scalar potential:

$$\begin{aligned} V(H, \eta, S, \Phi) = & -\mu^2 \tilde{H} \cdot H + m_\eta^2 \tilde{\eta} \cdot \eta + m_\Phi^2 |\Phi|^2 - \mu_S^2 |S|^2 - [\mu_c \tilde{\eta} \cdot H \Phi + \text{h.c.}] \\ & + \frac{1}{2} \lambda_1 (\tilde{H} \cdot H)^2 + \frac{1}{2} \lambda_2 (\tilde{\eta} \cdot \eta)^2 + \lambda_3 \tilde{H} \cdot H \tilde{\eta} \cdot \eta + \lambda_4 \tilde{H} \cdot \eta \tilde{\eta} \cdot H + \frac{1}{2} \lambda_5 |S|^4 \\ & + \lambda_6 \tilde{H} \cdot H |S|^2 + \lambda_7 |S|^2 \tilde{\eta} \cdot \eta + \frac{1}{2} \lambda_8 |\Phi|^4 + \lambda_9 |\Phi|^2 \tilde{H} \cdot H \\ & + \lambda_{10} |\Phi|^2 |S|^2 + \lambda_{11} |\Phi|^2 \tilde{\eta} \cdot \eta, \end{aligned} \quad (5)$$

where μ_k, m_j, λ_i are real parameters and $\tilde{H} = (0, -\frac{1}{\sqrt{2}}(v+h))^T$.

A. Symmetry breaking and the fermion-scalar spectrum

In this model, the vacuum expectation value (VEV) $\langle S \rangle = v_s/\sqrt{2}$ of the new scalar field, $S = (S^0 + v_s)/\sqrt{2}$, spontaneously breaks the new $U(1)_D$ Abelian gauge symmetry and yields

Dirac mass terms for the new dark fermions of the model $\chi_R, \chi_L, \psi_{Ri}, \psi_{Lj}$. In addition, the Higgs field develops its VEV, $\langle H \rangle = v/\sqrt{2}$, with $v = 246.2$ GeV. Consequently, according to the scalar potential (5), the Higgs H and the scalar S mix to form two mass eigenstates. In the basis (h^0, S^0) , the mass matrix reads

$$m_h^2 = \begin{pmatrix} -\mu^2 + \frac{1}{2}\lambda_6 v_s^2 - \frac{3\lambda_1 v^2}{2} & \lambda_6 v v_s \\ \lambda_6 v v_s & -\mu_s^2 + \frac{3}{2}\lambda_5 v_s^2 + \frac{\lambda_6 v^2}{2} \end{pmatrix}, \quad (6)$$

which is diagonalized by a unitary transformation $Z_H m_h^2 Z_H^T = m_{h,\text{diag}}^2$, such that:

$$\begin{pmatrix} h_0 \\ S^0 \end{pmatrix} = Z_H \begin{pmatrix} h_1 \\ h_2 \end{pmatrix} = \begin{pmatrix} \cos \theta & \sin \theta \\ -\sin \theta & \cos \theta \end{pmatrix} \begin{pmatrix} h_1 \\ h_2 \end{pmatrix}, \quad (7)$$

as described in Appendix B.

Similarly, after the electroweak and $U(1)_D$ symmetry breaking, the CP-even part η^0 of the η scalar doublet and Φ mix to form two mass eigenstates. In the basis (η^0, Φ) , the Lagrangian reads

$$\mathcal{L} = \Xi^T m^2 \Xi = \begin{pmatrix} \eta^0 & \Phi \end{pmatrix} \begin{pmatrix} m_\eta^2 + \frac{1}{2}\lambda_7 v_s^2 + \frac{1}{2}\lambda_3 v^2 + \frac{1}{2}\lambda_4 v^2 & -\frac{1}{2}v\mu_c \\ -\frac{1}{2}v\mu_c & m_\Phi^2 + \frac{1}{2}\lambda_{10} v_s^2 + \frac{1}{2}\lambda_9 v^2 \end{pmatrix} \begin{pmatrix} \eta^0 \\ \Phi \end{pmatrix}, \quad (8)$$

where the mass matrix m_Ξ^2 can be diagonalized via an orthogonal transformation

$$U_\Xi m_\Xi^2 U_\Xi^T = (m_\Xi)^{\text{diag}} = \text{diag}(m_1, m_2), \quad (9)$$

with

$$U_\Xi = \begin{pmatrix} \cos \theta_\Xi & \sin \theta_\Xi \\ -\sin \theta_\Xi & \cos \theta_\Xi \end{pmatrix}. \quad (10)$$

Regarding the fermion spectrum, in this model, we have two DM particles (DM1 and DM2) that are connected by the dark photon Z' and the Higgs portal S as is shown in Fig. 1. According to the Lagrangian 4 and after electroweak and $U(1)_D$ symmetry breaking, we get a Dirac fermion dark matter candidate, $\Psi_1 = (\chi_L, \chi_R)^T$, with mass $m_{\Psi_1} = y_c \frac{v_s}{\sqrt{2}}$. A second DM particle is the lightest eigenstate of two Dirac fermions (Ψ_2^1, Ψ_2^2) that result from the mixing of the four chiral fermions ψ_R^i and ψ_L^j ($i, j = 1, 2$). Therefore, the Lagrangian in the

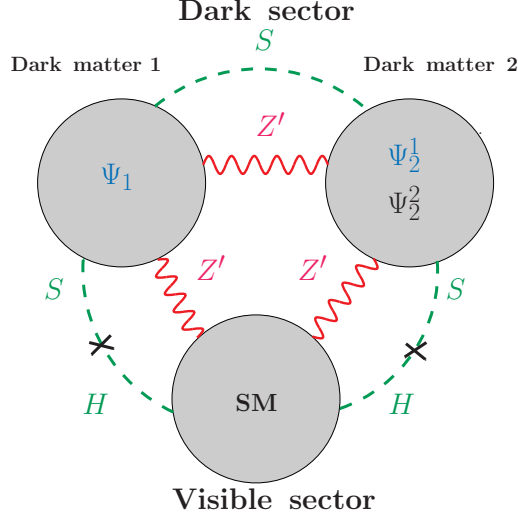


Figure 1. A schematic picture that shows our model setup with two secluded DM particles. Ψ_1 and Ψ_2^1 are the DM candidates. The dark photon Z' and the dark Higgs S mediate interactions between the two dark matter particles. In the case of a non-zero mixing angle between the scalars that acquire VEV or kinetic mixing, the dark sector also interacts with the visible sector.

mass eigenstate basis includes:

$$\mathcal{L} \supset m_{\Psi_1} \bar{\Psi}_1 \Psi_1 + \sum_{i=1}^2 m_{\Psi_2^i} \bar{\Psi}_2^i \Psi_2^i, \quad (11)$$

where Ψ_1 and Ψ_2^1 are the two DM particles in the model (we assume that Ψ_2^2 is heavier than Ψ_2^1). Notice that the fermions Ψ_2^i correspond to the eigenstates that are obtained after the diagonalization of the mass matrix $m_\psi = (Y_x)^{ij} \frac{v_s}{\sqrt{2}}$ with a biunitary transformation (Z_R, Z_L) such that $(m_{\Psi_2})^{\text{diag}} = \text{diag}(m_{\Psi_2^1}, m_{\Psi_2^2}) = Z_L m_\psi Z_R^\dagger$ as described in Appendix A. Finally, we have neutrino masses by realizing the effective Dirac neutrino masses operator shown in Eq. (2) (with $\delta = 1$). The specific realization is shown in Fig. 2 and, in Appendix A, we obtain all the Yukawa couplings in this Feynman diagram that are compatible with neutrino oscillation data to 3σ [18].

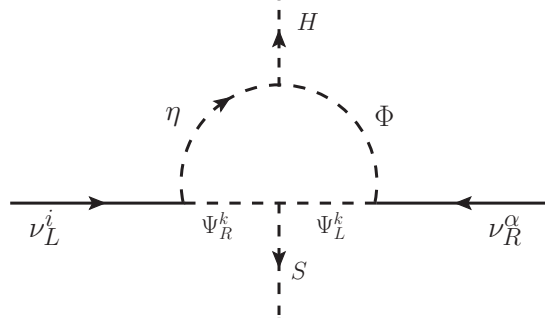


Figure 2. Feynman diagram for neutrino masses to one-loop.

B. Kinetic mixing and the electroweak gauge bosons

This model has a new gauge boson B'_μ associated with the $U(1)_D$ gauge symmetry. It interacts with the SM sector via kinetic mixing ϵ parameter. The Lagrangian for B'_μ reads

$$\begin{aligned} \mathcal{L}_{B'} = & -\frac{1}{4}B'_{\mu\nu}B'^{\mu\nu} - \frac{\epsilon}{2}B'_{\mu\nu}B^{\mu\nu} + \frac{i}{2}\bar{\Psi}_1\gamma^\mu(a_1 + b_1\gamma^5)B'_\mu\Psi_1 \\ & + \frac{i}{2}\sum_{k=1}^2\bar{\Psi}_2^k\gamma^\mu(a_2 + b_2\gamma^5)B'_\mu\Psi_2^k + (\mathcal{D}_\mu^X X)^\dagger\mathcal{D}^{X\mu}X + 9i\sum_{\alpha=1}^2\bar{\nu}_\alpha\gamma^\mu(1 + \gamma^5)B'_\mu\nu_\alpha, \end{aligned} \quad (12)$$

where, $a_k = (q_{\psi_L^k} - q_{\psi_R^k})$, $b_k = (q_{\psi_L^k} + q_{\psi_R^k})$, $B'_{\mu\nu} = (\partial_\mu B'_\nu - \partial_\nu B'_\mu)$, $B_{\mu\nu} = (\partial_\mu B_\nu - \partial_\nu B_\mu)$ are the strength tensors for B'_μ and B_μ respectively, and

$$\mathcal{D}_\mu^X = \partial_\mu - iq_X g_D B'_\mu, \quad (13)$$

for $X = S, \Phi, \eta$ and q_X are the charges under $U(1)_D$ gauge symmetry, g_D is the new $U(1)_D$ gauge coupling and the ν_α are Dirac neutrinos. In the basis $V_\mu = (B_\mu, W_\mu^3, B'_\mu)^T$, the mass matrix for the neutral gauge bosons reads [19]

$$\mathcal{L}_M = \frac{1}{2}V^{T\mu}M_G^2V_\mu, \quad (14)$$

where

$$M_G^2 = \frac{1}{4}v^2 \begin{pmatrix} g_1^2 & -g_1g_2 & -g_1^2\epsilon \\ -g_1g_2 & g_2^2 & g_1g_2\epsilon \\ -g_1^2\epsilon & g_1g_2\epsilon & 324g_D^2\frac{v_s^2}{v^2} + g_1^2\epsilon^2 \end{pmatrix}. \quad (15)$$

After the diagonalization of this matrix, we have three eigenstates. Those are the massless γ photon, the SM Z gauge boson with a mass $m_Z \approx 91.1$ GeV, and the new dark photon Z' with a mass $m_{Z'} \approx 9g_D v_s / (1 + \epsilon^2)$.

IV. DARK MATTER FREEZE-OUT

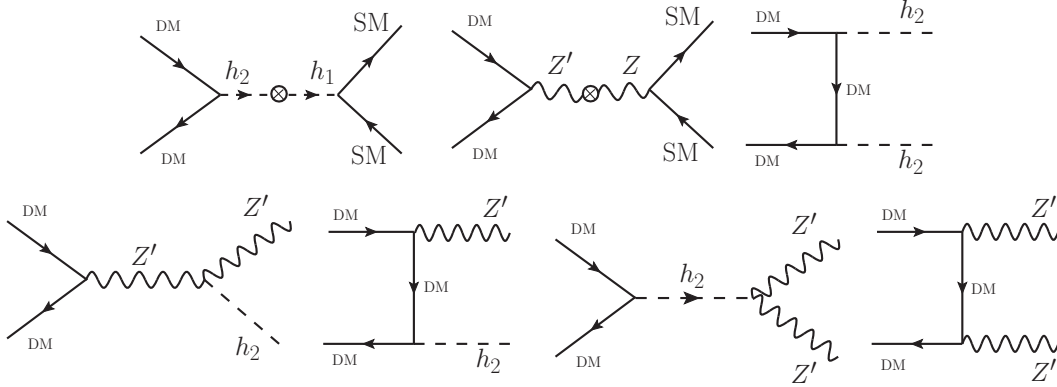


Figure 3. DM(Ψ_1, Ψ_2^1) annihilation channels (we do not show the corresponding u-channels.). The DM annihilation into SM model particles via mass mixing of the scalars h_i or kinetic mixing is extremely suppressed.

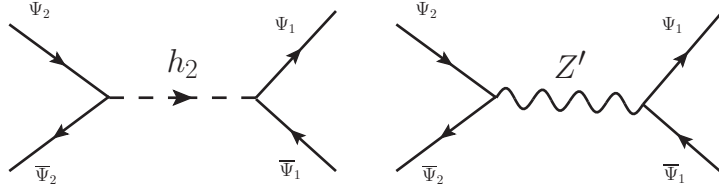


Figure 4. DM conversion channels $\Psi_1 \leftrightarrow \Psi_2^1$ mediated by the dark Higgs h_2 or the dark photon Z' .

In this model, the $U(1)_D$ dark symmetry determines the types of processes that render the relic abundance of DM. In Fig. 3, we show the direct annihilation into SM particles, Dirac neutrinos, the dark Higgs h_2 , and the dark photon Z' . Also, we show the DM conversion processes in Fig. 4.

The complete set of $2 \rightarrow 2$ processes that contribute to the relic density of DM can be classified by four digits [20]). For example, 0 is used for SM particles including the Z' and the h_2 fields, 1 for the Ψ_1 and $\bar{\Psi}_1$, 2 for Ψ_2 and $\bar{\Psi}_2$. For instance, the processes that are classified in the type 1100 have two SM particles in the final state and a pair $\Psi_1, \bar{\Psi}_1$ in the initial state. Notice that the $U(1)_D$ dark symmetry forbids the semi-annihilation process

as 1120 (only one SM particle) and the conversion process as 1112. Table II shows all the processes that contribute to the relic density of DM with their respective classification.

Processes	Type
$\bar{\Psi}_1 \Psi_1 \rightarrow \text{SM SM}$	1100
$\bar{\Psi}_2^1 \Psi_2^1 \rightarrow \text{SM SM}$	2200
$\bar{\Psi}_1 \Psi_1 \rightarrow \bar{\Psi}_2^1 \Psi_2^1$	1122
$\bar{\Psi}_2^1 \Psi_2^1 \rightarrow \bar{\Psi}_1 \Psi_1$	2211

Table II. The $2 \rightarrow 2$ processes allowed in this model that can modify the relic density of DM particles.

The relic abundance of DM Ω_i ($i = 1, 2$) for (Ψ_1, Ψ_2^1) is obtained by solving the Boltzmann equations:

$$\begin{aligned} \frac{d n_1}{d t} &= -\sigma_v^{1100}(n_1^2 - \bar{n}_1^2) - \sigma_v^{1122} \left(n_1^2 - n_2^2 \frac{\bar{n}_1^2}{\bar{n}_2} \right) - 3H n_1, \\ \frac{d n_2}{d t} &= -\sigma_v^{2200}(n_2^2 - \bar{n}_2^2) - \sigma_v^{2211} \left(n_2^2 - n_1^2 \frac{\bar{n}_2^2}{\bar{n}_1} \right) - 3H n_2, \end{aligned} \quad (16)$$

where n_i ($i = 1, 2$) is the number density for the DM particle, \bar{n}_i are their respective equilibrium values and σ_v^{abcd} is the thermally averaged cross section, that satisfies the relation $\bar{n}_a \bar{n}_b \sigma_v^{abcd} = \bar{n}_c \bar{n}_d \sigma_v^{cdab}$.

In the next section, we compute the analytical expression for the relic density in a simplified regime. However, in this work, we used `micrOMEGAs 6.0.3` [21] to compute Ω_i because it considers all the processes involved in the thermal evolution of the coupled Boltzmann eqs. (16). We define the following parameters for the DM particles that allow us to study the relevant processes that play a role in the evolution of the Boltzmann equations and consequently affect the relic abundance of DM:

$$\zeta_{anni}^i(T) = \frac{\sigma_v^{ii00}(T)}{\sigma_v^{ii00}(T) + \sigma_v^{iijj}(T)} \quad (17)$$

$$\zeta_{conv}^i(T) = \frac{\sigma_v^{iijj}(T)}{\sigma_v^{ii00}(T) + \sigma_v^{iijj}(T)}, \quad (18)$$

$i \neq j = 1, 2$, where those parameters are evaluated at the typical freeze-out temperature: $T \approx m_{\chi_1}/25$. Notice that by construction, $\zeta_{anni}^i + \zeta_{conv}^i = 1$, and for example: $\zeta_{anni}^1 \approx 1$

means that the relic density of Ψ_1 particle is dominated by the annihilation process 1100 and the conversion 1122 (2211) contributions are negligible. In practice, to compute those parameters we used the specific function `vsabcdF(T)` incorporated into the last version of `micrOMEGAs 6.0.3` [21], which allows us to evaluate the cross sections $\sigma_v^{ijj}, \sigma_v^{ii00}$ at some specific temperature.

Finally, we impose the constraint:

$$\Omega h^2 = \Omega_1 h^2 + \Omega_2 h^2 = 0.1200 \pm 0.0012, \quad (19)$$

where Ωh^2 is the observed value by the PLANCK experiment [22]. Notice that, experimental signals of DM in any detector are affected by the fraction of the local abundance of the DM candidate. This fraction is defined as:

$$\xi_i = \frac{\Omega_i}{\Omega}, (i = 1, 2), \quad (20)$$

such that $\xi_1 + \xi_2 = 1$. This feature distinguishes between a case with one single-component DM candidate and a multicomponent scenario.

Since the dark sector is in thermal equilibrium, the abundance of DM is determined by the thermal freeze-out into lighter hidden particles h_2 and Z' as shown in Fig. 3. Notice that h_2 is a new Higgs scalar that could be detected in high energy experiments. Also, notice that the dark photon Z' is unstable because it decays into Dirac neutrinos with a decay width

$$\Gamma_{Z' \rightarrow \bar{\nu}_i \nu_i} = 3 M_{Z'} \frac{(g_1^2 \epsilon^2 + 4 q_{\nu_R}^2 g_D^2)}{64\pi}, \quad (21)$$

where $q_{\nu_R} = 9$ is the charge of the right-handed neutrino (see Tab. I). Experimentally, the dark photon Z' needs to decay in less than one second, $1/\Gamma \lesssim 1$ sec, and is absent at the time of Big Bang Nucleosynthesis (BBN) [1]. Since left-handed and right-handed neutrinos are in two different sectors in the early Universe, the decay of Z' does not reheat SM plasma. Notice that our model could render the relic abundance of DM compatible with BBN even without the kinetic mixing parameter [23–25]. Also, cosmological constraint due to the contribution of right-handed neutrinos to relativistic degrees of freedom in the early Universe is satisfied as shown in appendix F. Thus, a fully consistent scenario, even without kinetic mixing, is compatible with all theoretical, cosmological, and phenomenological

constraints. Finally, we emphasize that at low temperatures, left-handed and right-handed neutrinos mix to form Dirac neutrinos in a process known as “left-right equilibration” [26].

A. One-component WIMP Limit

As a benchmark scenario, suppose that $m_{Z'} < m_{\Psi_1} \ll m_{\Psi_2^1}$, the kinetic mixing and the mixing angles θ in the scalar sector are zero, and $m_{h_2} > 2m_{\Psi_1} \gg 125$ GeV. In this scenario, Boltzmann eqs. (16) disentangle, and the relic density associated with the DM particle that has only one generation dominates the total relic density ($\zeta_{conv}^1 \rightarrow 0$). In this scenario, the DM abundance is rendered by secluded thermal freeze-out, through $\bar{\Psi}_1 \Psi_1 \rightarrow Z' Z'$ processes shown in Fig. 3 (notice that $\bar{\Psi}_1 \Psi_1 \rightarrow Z' h_2$ is forbidden by kinematics).

In this limit, the thermal evolution of Ψ_1 follows the freeze-out mechanism in the dark sector. As the Universe adiabatically cooled down, the Universe’s expansion overtook the DM annihilation rate $\Gamma \ll H$, and the relic density of DM was frozen out. The Boltzmann eqs. (16), yields [27, 28]

$$\Omega_1 h^2 \approx \frac{2.08 \times 10^9 x_f \text{ GeV}^{-1}}{M_{\text{Pl}} \sqrt{g_*(T_f)} (a + 3b/x_f)}, \quad (22)$$

where the parameters a and b comes from the thermally-averaged annihilation cross-section $\langle \sigma v \rangle = (a + bv^2 + \mathcal{O}(v^4))$, $g_*(T)$ is the effective number of degrees of freedom at the temperature T , $x_f = m_{\Psi_1}/T_{\text{freeze-out}}$ and where h is today’s Hubble parameter in units of 100 km/s/Mpc. Also, in this limit, the thermally averaged annihilation cross section is given by (see Eq.(C3)):

$$\langle \sigma v \rangle \approx \frac{g_D^4 (1 - r^2)^{3/2} (1519 r^2 + 162)}{16 \pi m_{\Psi_1}^2 r^2 (r^2 - 2)^2} + b v^2, \quad (23)$$

with $r = m_{Z'}/m_{\Psi_1}$ and the p-wave is given by Eq.(C4).³

In Fig. 5, we show the behavior of the relic abundance $\Omega_1 h^2$ given by the Eq. (22) as a function of the dark photon mass $m_{Z'}$. We choose the benchmark scenario with $m_{\Psi_2^1} = 1000$ GeV, $m_{\Psi_2^2} = 2000$ GeV, $y_c = 0.85$, $v_s = 400$ GeV, $1 < m_{Z'}/\text{GeV} < 100$ and $m_{h_2} = \{550, 553, 558\}$ GeV. The black star in Fig. 5 is the benchmark point for $m_{Z'} \approx 43$

³ In the appendix C we computed the $\langle \sigma v \rangle$ with FeynArts 3.11 [29] and FeynCalc 10.0.0 [30–32]. We obtained a general expression that matches the vector-like limit studied in Refs. [1, 2, 11, 33] and the axial-vector case in Refs.[9, 34, 35]

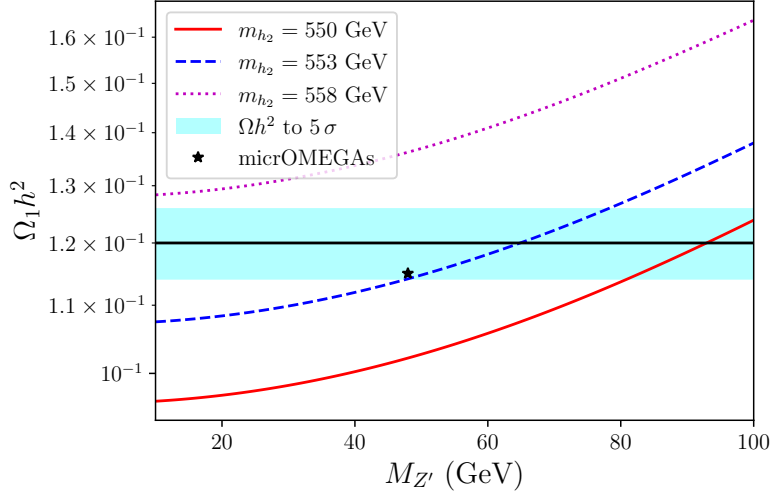


Figure 5. Relic density in the limit of one DM component Ψ_1 .

GeV and $m_{h_2} = 553$ GeV, computed with `micrOMEGAs` that shows a good agreement with the limit of one DM component. For this point $\langle\sigma v\rangle \approx 3 \times 10^{-26}$ cm³/s.

V. PHENOMENOLOGY OF THE MODEL

We implemented this model in `SARAH` [36–40], and coupled it with the `SPheno` [41, 42] routines to obtain the spectrum of the model. We computed the DM relic density using `micrOMEGAs` 6.0.3 [21] that numerically solves the coupled set of Boltzmann eqs. (16) for the two DM candidates. We selected the points in the parameter space compatible with the current value of the DM relic density in eq. (19) and the neutrino masses (see Appendix A). We also considered the constraints due to the branching ratio of Higgs and Z boson decays into invisible as shown in Appendices D, E. The branching ratios of the decays of Higgs and Z bosons into invisible particles are many orders of magnitude below the current constraint and do not affect our model’s parameter space. However, cosmological constraints due to the effective number of relativistic degrees of freedom in the early Universe constrain the value of the kinetic mixing of the model as shown in Appendix F.

We randomly scanned the model’s parameter space by varying the parameters as shown in Table III. The parameters in the model were chosen as real. We fixed the SM Higgs mass $m_{h_1} = 125$ GeV, $m_{h_2} > m_{h_1}$ and $\lambda_1, \lambda_5, \lambda_6$ were computed in terms of the mixing

Parameter	Range
$M_{Z'}/\text{GeV}$	$1 - 10^3$
g_D	$10^{-3} - 1$
y_c	$10^{-3} - 1$
$(m_{\Psi_2^j} - m_{\Psi_1})/\text{GeV}$	$1 - 5 \times 10^3$
θ	$10^{-6} - 10^{-3}$
θ_L, θ_R	$10^{-3} - 2\pi$
λ_k	$10^{-4} - 1$
m_{h_2}/GeV	$125 - 5 \times 10^3$
m_η^2/GeV^2	$10^6 - 10^8$
m_Φ^2/GeV^2	$10^6 - 10^8$
μ_c/GeV	$10^2 - 2 \times 10^3$
ϵ	$10^{-12} - 10^{-2}$
y_{nL}	$10^{-4} - 1$

Table III. Scan ranges for the free parameters in this model. $k = \{2, \dots, 11\}$, $k \neq \{5, 6\}$, $j = 1, 2$.

angle θ as described in the appendix B. According to collider constraints, it follows that $|\sin \theta| < 0.3$ for $m_{h_2} > m_{h_1}$ [43–46]. However, in this work, we considered $10^{-6} < \theta < 10^{-3}$ which suppresses the dark Higgs portal for direct detection of DM. This value for θ was motivated because the DM is a Dirac particle in this model, and the vector portal is open for direct detection. For Majorana DM, instead the dark Higgs portal is the only open channel for direct detection as shown in Ref. [47]. Also, the Yukawa couplings $(y_x)^{ij}$ in Eq. (4) were computed in terms of $m_{\Psi_1^j}, m_{\Psi_2^j}$ and the mixing angles $\theta_{L,R}$ as described Appendix A. Finally, the Yukawa couplings $(y_{nR})^{\alpha i}$ in Lagrangian (4) were parameterized in terms of the $(y_{nL})^{i\alpha}$ Yukawa couplings, the neutrino masses $m_{\nu\alpha}$ and the Pontecorvo-Maki-Nakagawa-Sakata matrix [48] as described in Appendix A. In this model, the new Yukawa couplings reproduce the current neutrino oscillation data by construction [18].

In this paper, we study only the case of fermionic DM. Fig. 6 shows the behavior of the DM relic density for the two fermionic DM candidates. Notice that our model can render DM relic abundance for masses that range between 1 GeV to the TeV scale. Each fermionic

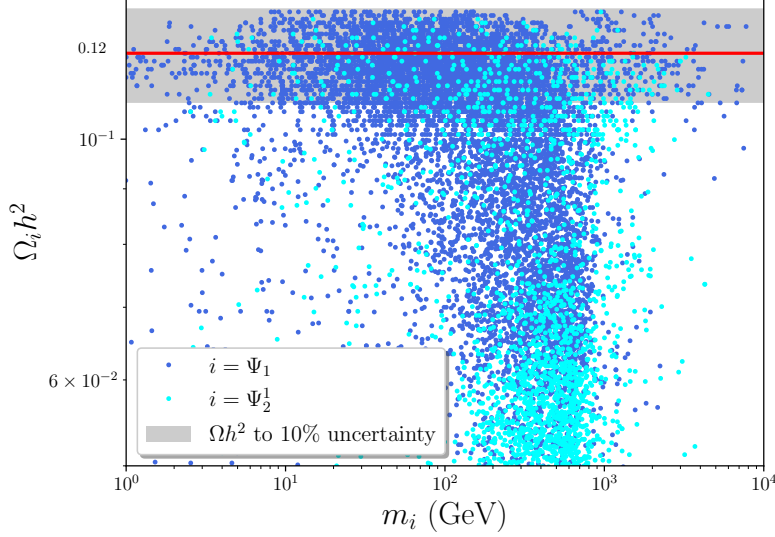


Figure 6. DM relic density for the two fermionic DM candidates (Ψ_1, Ψ_2^1).

DM candidate (Ψ_1, Ψ_2^1) could render the 100% of the DM abundance, those are the points in the grey horizontal band with 10% of uncertainty and $\xi_i = (\Omega_i/\Omega) \approx 1$. In addition, the interaction between the two candidates for DM gives the value $\Omega h^2 \approx 0.12$ [22]. They correspond to the models below the grey band with $\xi_i = (\Omega_i/\Omega) \leq 1$, but $\xi_1 + \xi_2 = 1$. Also, we realize that for a DM masses bigger than $m_{Z'}$, the process $\bar{\Psi}\Psi \rightarrow Z'Z'$ is kinematically favored and domains the scan with a branching near to one (as shown in s, u and t-channels in Fig. 3). In contrast, a DM particle lighter than $m_{Z'}$ decays directly into SM fermions, preferably into two Dirac neutrinos $\bar{\Psi}\Psi \rightarrow \bar{\nu}_i\nu_i$ ($i = 1, 2, 3$).

Also, we study the DM conversion described by the Feynman diagram shown in Fig. 4. In Fig. 7 we show the effect of the type process 2211 in Tab. II. Notice that DM conversion $\bar{\Psi}_2\Psi_2 \rightarrow \bar{\Psi}_1\Psi_1$ is kinematically allowed because $m_{\Psi_1} < m_{\Psi_2^1}$ as we described in Tab. III. These plots show that the thermal annihilation cross section σ_v^{2211} in Boltzmann eqs. 16, which is included in the parameter $\zeta_{ann}^2(T)$, contributes significantly to the relic abundance of DM for some points of our DM model (green points).

In the left plot of Fig. 7 we show the behavior of the ζ_{ann}^2 parameter in the $|m_{\Psi_1} - m_{\Psi_2^1}|$ plane (see eq. 17). The relic abundance of DM is almost always dominated by annihilation processes directly to the SM particles where $\zeta_{ann}^2 \approx 1$ (yellow points). However, for the green darker points, the DM conversion process $\bar{\Psi}_2\Psi_2 \rightarrow \bar{\Psi}_1\Psi_1$ is relevant and the thermal cross

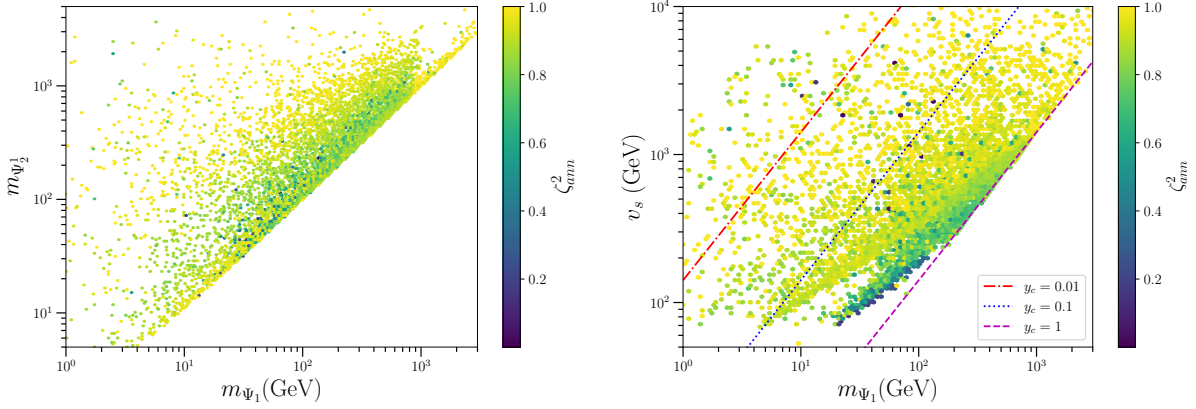


Figure 7. DM conversion impact. The green darker points represent models where the conversion thermal cross-section σ_v^{2211} significantly contributes to the relic abundance of DM.

section σ_v^{2211} plays an important role in rendering the relic abundance of DM. Also, in the right plot of Fig. 7 we show the behavior of the ζ_{ann}^2 parameter in the $|m_{\Psi_1} - v_s|$ plane. The Yukawa coupling y_c in the Lagrangian 4 not only determines the mass of the lightest DM particle but also plays an important role in the DM conversion process $\bar{\Psi}_2\Psi_2 \rightarrow \bar{\Psi}_1\Psi_1$ that directly impacts the relic abundance Ω_1 . This conversion process is activated principally for $y_c \gtrsim 0.1$ and $v_s \lesssim 1$ TeV (dark green points).

A. Direct and indirect detection of DM

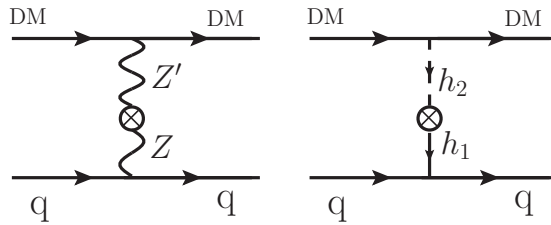


Figure 8. Spin independent interactions of DM (Ψ_1, Ψ_2^1) with nuclei: vector (left) and scalar (right) portals.

This model allows for direct detection signatures since the DM scatters with nuclei through the t-channel in the vector and scalar portal shown in Fig. 8. The contribution of

the vector portal (left) to the spin independent (SI) cross-section is given by [49, 50]

$$\sigma_{\Psi_i N}^{\text{SI-vector}} = \frac{\mu^2}{4\pi} \frac{g_D^2 g_1^2 \epsilon^2}{M_{Z'}^4} B_{\Psi_i}^2, \quad (24)$$

where $\mu = M_N m_{\Psi_i} / (M_N + m_{\Psi_i})$ is the reduced mass, $M_N \approx 939$ MeV is the nucleon mass (neutron or proton), $B_{\Psi_1} = (q_{\chi_L} - q_{\chi_R}) = 1$, $B_{\Psi_2} = (q_{\psi_L} - q_{\psi_R}) = 9$ (see Tab. I). On the other hand, the contribution of the scalar portal (right) to the spin SI cross-section is given by [45, 51]:

$$\sigma_{\Psi_i N}^{\text{SI-scalar}} = \frac{\mu^2}{2\pi} \left(\frac{y' \cos \theta \sin \theta}{v} \right)^2 \left(\frac{1}{m_{h_2}^2} - \frac{1}{m_{h_1}^2} \right)^2 f^2 M_N^2, \quad (25)$$

with the effective Higgs-nucleon coupling $f \approx 0.3$ and y' is the scalar coupling between the dark Higgs and the DM particle. After the scan was done, we noticed that the vector interaction was dominant. The scalar portal is subdominant because the Higgs mixing angle θ was chosen less than 10^{-3} in Table III. Note that although kinetic mixing ϵ plays an important role in the direct detection of DM and opens the door to current and future searches of DM, it does not play a significant role in determining the relic abundance of DM in this secluded framework.

Fig. 9 shows the SI cross section for elastic scattering of DM with nuclei for each DM component of the model (Ψ_1 on the left and Ψ_2^1 on the right.). The SI scales with the parameter $\xi_i = \Omega_i / \Omega$ that accounts for the DM density fraction on Earth (see eq. (20)). After we scan the parameter space of the model for parameters that range as shown in Tab. III, we filter all the points (models) that fall under the current limit set by XENONnT experiment [52]. We also show the projected WIMP sensitivity of the LUX-ZEPLIN (LZ) experiment [53] and the prospects of the DARWIN experiment [54] that is one of the final next generation of DM experiments before reaching the threshold for Neutrino Coherent Scattering (NCS) [55, 56], where the neutrino-nuclei interaction mimics any DM signal on the detector (neutrino floor). In Fig. 9, the yellow points represent the viable models where both DM particles are expected to have signals in future experiments (points above the DARWIN experiment and below the current limit of XENONnT for the two DM components). Also, notice, that in this model, the neutrinos are Dirac particles and contribute to the number of relativistic degrees of freedom in the early Universe via the kinetic mixing parameter [17] (see Appendix F). In Fig. 9, the magenta region shows the models with

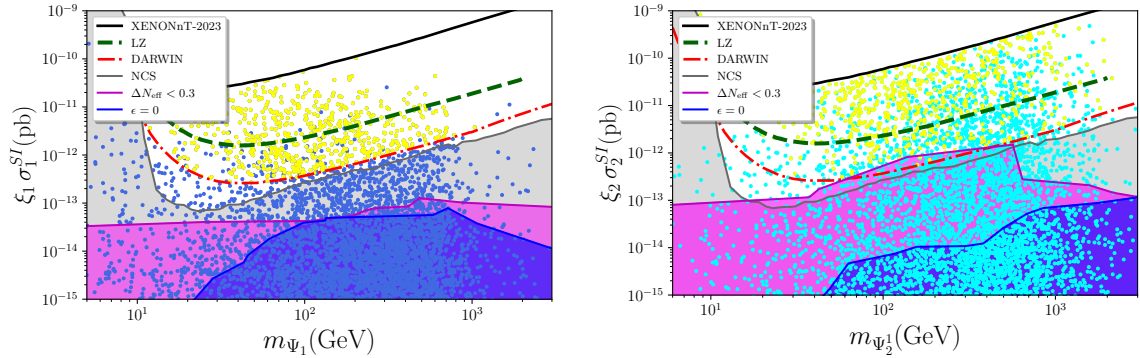


Figure 9. SI cross-section for elastic scattering of DM with nuclei scaled by ξ_i fraction of DM. We also show the limit set by XENONnT collaboration [52], the projected WIMP sensitivity from LZ [53] and DARWIN [54] experiments. Also, we show the Neutrino Coherent Scattering (NCS) [55, 56], the allowed region by the ΔN_{eff} (magenta color) and the region with $\epsilon = 0$ (blue color). Yellow points represent the viable models where both DM particles are expected to yield signals in future experiments.

$\Delta N_{\text{eff}} < 0.3$ (Planck+BAO combinations [22]). Also, we show the blue region where $\epsilon = 0$. Notice that it is inside the magenta region and represents the models with zero contribution to the relativistic degrees of freedom at tree level. However, although kinetic mixing could be generated radiatively [15], we check that it is always negligible in our model.

Finally, we also checked the spin-dependent (SD) WIMP-neutron cross-section with `micrOMEGAs 6.0.3`. We found that all models have a SD cross-section $\sigma^{\text{SD}} \leq 10^{-43} \text{ cm}^2$, that is below the experimental constraints of XENON1T [57] and its prospects as DARWIN [54] and LZ [53].

Fig. 10 studies the impact of the kinetic mixing parameter in the direct detection of DM. According to eq. (24), the vector SI cross-section is a function of kinetic mixing, the DM mass, and the new $U(1)_D$ gauge coupling g_D . Moreover, Fig. 10 shows some contours for the XENONnT current limit for some fixed values of the dark photon $m_{Z'}$ and gauge coupling g_D through the VEV v_s . Notice that low masses of the dark photon prefer low values for the kinetic mixing parameter (blue dashed line). Also, kinetic mixing values below 10^{-6} are not restricted by XENONnT current limit because the SI cross-section is always under the neutrino floor.

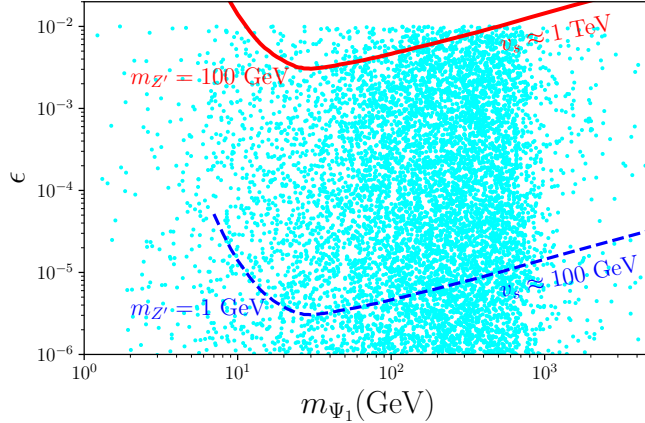


Figure 10. XENONnT contours limits for some dark photon masses projected in the plane of the kinetic mixing vs DM mass m_{Ψ_1} .

On the other hand, concerning the indirect detection of DM in this model, we performed an exhaustive numerical analysis with the `micrOMEGAs` program to compute today’s annihilation rate. We realized that the principal annihilation channels for Ψ_1 are (also apply for Ψ_2^1): $\bar{\Psi}_1\Psi_1 \rightarrow \bar{\nu}_i\nu_i$, $\bar{\Psi}_1\Psi_1 \rightarrow Z'Z'$, with a thermal average cross section $\langle\sigma v\rangle$ a little below the canonical value $\sim 3 \times 10^{-26} \text{ cm}^3/\text{s}$. However, the process involving the Z' triggers secondary particles in a 4-step cascade annihilation [58] where the unstable dark photon Z' decays in two states, principally in neutrinos $Z' \rightarrow \bar{\nu}_i\nu_i$. This process could enhance the neutrino flux. However, this is beyond the work’s scope. We also have the annihilation channel $\bar{\Psi}_1\Psi_1 \rightarrow h_2Z'$ where the extra scalar h_2 (Higgs-like) could decay in a leptonic or hadronic way with a significant modification of the gamma-ray spectrum, as analyzed in Ref. [59]. Finally, we also have direct annihilation channels (prompt channels) into two leptons $\bar{\Psi}_1\Psi_1 \rightarrow \bar{e}_ie_i$ and two light quarks $\bar{\Psi}_1\Psi_1 \rightarrow \bar{q}_iq_i$. However, in this model, these channels are suppressed by the kinetic mixing. After the scan shown in Tab. III, the $\langle\sigma v\rangle$ in these primary channels is under the value of $\sim 10^{-30} \text{ cm}^3/\text{s}$, which is almost three-four orders of magnitude below the current limits and prospects of Fermi-LAT [60] and the Cherenkov telescope arrays such as H.E.S.S [61], CTA [62], SWGO [63] (see Ref. [59] for more details).

During the completion of this work, a similar work on chiral dark matter and radiative neutrino masses from a gauged $U(1)$ symmetry appears [47]. There, with an alternative

method to find some solutions, they explored a subset where all chiral fermions acquire masses after SSB. Without massless right-handed neutrinos, they generate scotogenic Majorana neutrino masses, and in our limit of a decoupled inert scalar sector, they need the kinetic mixing to explain the full DM phenomenology.

VI. CONCLUSIONS

This paper shows a complete UV realization of a secluded WIMP dark matter model with an extra Abelian gauge symmetry that includes two-component dark matter candidates, where Dirac neutrino masses are generated at one-loop via a scotogenic realization of the effective operator for Dirac neutrino masses in the SM. Our paper explains the relic abundance of dark matter, even without kinetic mixing. Also, it can be tested in direct detection experiments like DARWIN. However, the annihilation of dark matter particles into gamma rays is highly suppressed due to the dark nature of the Abelian gauge symmetry. The model's parameter space explains the relic abundance of DM and Dirac neutrino masses. It is also compatible with cosmological and theoretical constraints, including the branching ratio of SM into invisible, BBN restrictions, and the number of relativistic degrees of freedom in the early Universe, even without kinetic mixing.

VII. ACKNOWLEDGMENTS

We thank Walter Tangarife for their enlightening discussions and reading of the manuscript. This work have been supported by Sostenibilidad UdeA, UdeA/CODI Grants 2022-52380 and 2023-59130, Minciencias Grants CD 82315 CT ICETEX 2021-1080.

Appendix A: Dirac Neutrino Masses

In this model, we have a scotogenic realization of an effective operator for Dirac neutrino masses [3]:

$$\mathcal{L}_{\text{eff}} = Y_\nu^{\alpha i} (\nu_{R\alpha})^\dagger L_i \cdot \tilde{H} \left(\frac{S^*}{\Lambda} \right)^\delta + \text{h.c.}, \quad (\text{A1})$$

where $\delta = 1$, (\cdot) is the $SU(2)_L$ dot product, $\tilde{H} = (0, -\frac{1}{\sqrt{2}}(v+h))^T$ and Λ is the energy scale where Dirac mass terms for neutrinos are generated. After spontaneous symmetry breaking, the mass Lagrangian for fermions in the dark sector that have two generations is:

$$\mathcal{L} = \frac{v_s}{\sqrt{2}} \begin{pmatrix} \psi_L^1 & \psi_L^2 \end{pmatrix} \begin{pmatrix} y_x^{11} & y_x^{12} \\ y_x^{21} & y_x^{22} \end{pmatrix} \begin{pmatrix} \psi_R^1 \\ \psi_R^2 \end{pmatrix} + \text{h.c.} = \psi_L^T m_\psi \psi_R + \text{h.c.}, \quad (\text{A2})$$

where the matrix m_ψ is diagonalized as:

$$Z_L m_{\psi_2} Z_R^\dagger = (m_\psi)^{\text{diag}} = \text{diag}(m_{\Psi_1^2}, m_{\Psi_2^2}) \quad (\text{A3})$$

with

$$Z_{L,R} = \begin{pmatrix} \cos \theta_{L,R} & \sin \theta_{L,R} \\ -\sin \theta_{L,R} & \cos \theta_{L,R} \end{pmatrix}. \quad (\text{A4})$$

We realize an effective Dirac neutrino mass operator via a scotogenic mechanism at one loop (see Feymann diagram 2). At one loop level, we obtain a neutrino mass matrix:

$$(\mathcal{M}_\nu)^{\alpha\beta} = \frac{1}{(4\pi)^2} \sum_{k=1}^2 \sum_{l=1}^2 \sum_{r=1}^2 (y_{nL})^{\alpha k} (y_{nR})^{\beta r} (Z_R)^{kl} (Z_L)^{rl} M_l [U_\Xi^{11} f(m_1, M_l) U_\Xi^{21} + U_\Xi^{12} f(m_2, M_l) U_\Xi^{22}], \quad (\text{A5})$$

which can be written as

$$(\mathcal{M}_\nu)^{\alpha\beta} = \sum_{k=1}^2 \sum_{r=1}^2 (y_{nL})^{\alpha k} f^{kr} (y_{nR})^{\beta r}, \quad (\text{A6})$$

where

$$f^{kr} = \frac{1}{(4\pi)^2} \sum_{l=1}^2 Z_R^{kl} Z_L^{rl} M_l [U_\Xi^{11} f(m_1, M_l) U_\Xi^{21} + U_\Xi^{12} f(m_2, M_l) U_\Xi^{22}], \quad (\text{A7})$$

$$f(m_i, M_l) = \frac{m_i^2 \ln(m_i^2) - M_l^2 \ln(M_l^2)}{m_i^2 - M_l^2}. \quad (\text{A8})$$

We rotate to mass eigenstates from flavor eigenstates by using a biunitary transformation

$$M_{\text{diag}}^\nu = U^\dagger M^\nu V, \quad (\text{A9})$$

where U is the neutrino mixing matrix PMNS [48], V is a unitary transformation matrix for right-handed neutrinos. The eigenvalues for neutrino masses can be related to data from PDG [64] (we consider normal hierarchy)

$$m_{\nu_1} \equiv 0, \quad (\text{A10})$$

$$m_{\nu_2} \equiv \sqrt{\Delta m_{21}^2} = 8.678 \times 10^{-12} \text{ GeV}, \quad (\text{A11})$$

$$m_{\nu_3} \equiv m_{\nu_2} + \sqrt{\Delta m_{23}^2} = 5.01 \times 10^{-11} \text{ GeV}. \quad (\text{A12})$$

In this paper, we consider the parameters $(y_{nL})^{\alpha k}$ as free parameters (We consider $(y_{nL})^{11} = 0$ and $(y_{nL})^{12} = 0$). Then, we write the couplings y_{nR} in terms of neutrino observables

$$(y_{nR})^{i1} = -\frac{(y_{nL})^{32} m_{\nu_2} U^{i2} - (y_{nL})^{22} m_{\nu_3} U^{i3}}{[(y_{nL})^{22} (y_{nL})^{31} - (y_{nL})^{21} (y_{nL})^{32}] \Lambda_1}, \quad (\text{A13})$$

$$(y_{nR})^{i2} = -\frac{(y_{nL})^{31} m_{\nu_2} U^{i2} - (y_{nL})^{21} m_{\nu_3} U^{i3}}{[(y_{nL})^{22} (y_{nL})^{31} - (y_{nL})^{21} (y_{nL})^{32}] \Lambda_2}, \quad (\text{A14})$$

where

$$\Lambda_j = Z_R^{j1} Z_L^{j1} \mathcal{F}^1 + Z_R^{j2} Z_L^{j2} \mathcal{F}^2, \quad (\text{A15})$$

$$\mathcal{F}^k = m_{\Psi_2^k} (Z_N^{11} f(m_1, m_{\Psi_2^k}) Z_N^{21} + Z_N^{12} f(m_2, m_{\Psi_2^k}) Z_N^{22}), \quad (\text{A16})$$

for $i = 1, 2, 3$ and $j, k = 1, 2$.

Appendix B: Diagonalization

After EWSB and SSB, we solve the tadpole equations and obtain the mass matrix

$$m_h^2 = \begin{pmatrix} \lambda_1 v^2 & \lambda_6 v v_s \\ \lambda_6 v v_s & \lambda_5 v_s^2 \end{pmatrix}, \quad (\text{B1})$$

that is diagonalized via an orthogonal matrix:

$$U = \begin{pmatrix} \cos \theta & \sin \theta \\ -\sin \theta & \cos \theta \end{pmatrix}, \quad (\text{B2})$$

where $U^T M U = M_{\text{diagonal}}$ and

$$M_{\text{diagonal}} = \begin{pmatrix} m_{h_1}^2 & 0 \\ 0 & m_{h_2}^2 \end{pmatrix}. \quad (\text{B3})$$

We can write the λ_1 , λ_5 , and λ_6 couplings can be written in terms of the mixing angle θ and the eigenvalues $m_{h_{1,2}}$ as

$$\lambda_1 = \frac{1}{2v^2} \left(m_{h_1}^2 + m_{h_2}^2 - \frac{(m_{h_2}^2 - m_{h_1}^2)}{\sqrt{1 + \tan^2(2\theta)}} \right), \quad (\text{B4})$$

$$\lambda_5 = \frac{1}{2v_s^2} \left(m_{h_1}^2 + m_{h_2}^2 + \frac{(m_{h_2}^2 - m_{h_1}^2)}{\sqrt{1 + \tan^2(2\theta)}} \right), \quad (\text{B5})$$

$$\lambda_6 = \frac{1}{2vv_s} \frac{m_{h_2}^2 - m_{h_1}^2}{\sqrt{1 + \tan^2(2\theta)}} \tan(2\theta). \quad (\text{B6})$$

Appendix C: General thermal annihilation cross-section

The thermally averaged cross section for DM annihilation for the process $\Psi\bar{\Psi} \rightarrow Z'Z'$ is written as powers of the relative velocity v as $\langle\sigma v\rangle = (a + bv^2 + O(v^4))$, where

$$a = \frac{g_D^4 (1 - r^2)^{3/2} (Q_A^4 r^2 + 2Q_A^2 Q_V^2 (4 - 3r^2) + Q_V^4 r^2)}{4\pi r^2 (r^2 - 2)^2 M_\Psi^2}, \quad (\text{C1})$$

$$b \approx \frac{g_D^4}{384\pi m_\Psi^2 (m_h^2 - 4m_\Psi^2)^2} \left[\frac{8(-8(4Q_A^2 + 81)Q_V^2 m_h^2 m_\Psi^2 + 4Q_A^2 Q_V^2 m_h^4 + m_\Psi^4 (32(2Q_A^2 + 81)Q_V^2 + 59049))}{r^2} \right. \\ + r^2(-4m_h^2 m_\Psi^2 (32Q_A^4 + Q_A^2 (64Q_V^2 + 81) + Q_V^2 (32Q_V^2 + 81))) \\ + r^2(16m_h^4 (Q_A^2 + Q_V^2)^2) \\ + r^2(m_\Psi^4 (256Q_A^4 + 16Q_A^2 (32Q_V^2 + 81) + 256Q_V^4 + 1296Q_V^2 - 98415)) \\ + 2(-8m_h^2 m_\Psi^2 (3Q_A^4 + 6Q_A^2 (7Q_V^2 - 27) - 7Q_V^4 + 162Q_V^2)) \\ + 2(m_h^4 (3Q_A^4 + 42Q_A^2 Q_V^2 - 7Q_V^4)) \\ + 2(m_\Psi^4 (48Q_A^4 + 96Q_A^2 (7Q_V^2 - 54) - 112Q_V^4 + 5184Q_V^2 + 177147)) \\ \left. + \frac{16(-4Q_V^2 (4Q_V^2 + 81) m_h^2 m_\Psi^2 + 2Q_V^4 m_h^4 + (32Q_V^4 + 1296Q_V^2 + 19683) m_\Psi^4)}{r^4} \right], \quad (\text{C2})$$

with $r = m_{Z'}/m_\Psi$, $Q_A = (q_R - q_L)/2$ and $Q_V = (q_R + q_L)/2$ are the axial-vector and vector charges. q_L, q_R are the left and right Weyl fermion charges that form the Dirac fermion Ψ . The s-wave matches the expression in Refs.[9, 34, 35] and the p-wave is reported for the first time. Although those expressions are general, in this work, the lightest DM particle is Ψ_1 : with $q_L = 4, q_R = 5$ as is shown in Tab. I, and therefore, the s-wave and the p-wave contributions become:

$$a = \frac{g_D^4 (1 - r^2)^{3/2} (1519 r^2 + 162)}{16\pi m_\Psi^2 r^2 (r^2 - 2)^2}, \quad (\text{C3})$$

$$b \approx \frac{g_D^4}{384\pi m_\Psi^2 (m_h^2 - 4m_\Psi^2)^2} \left[\frac{16 \left(-13122m_h^2 m_\Psi^2 + \frac{6561m_h^4}{8} + 59049m_\Psi^4 \right)}{r^4} \right. \\ \left. - \frac{8 \left(-13284m_h^2 m_\Psi^2 + \frac{81m_h^4}{4} + 111861m_\Psi^4 \right)}{r^2} + r^2 \left(-60434m_h^2 m_\Psi^2 + 6724m_h^4 + 35737m_\Psi^4 \right) \right. \\ \left. + 2 \left(-4659m_h^2 m_\Psi^2 - \frac{21261m_h^4}{8} + 238305m_\Psi^4 \right) \right]. \quad (\text{C4})$$

Note that in the vector-like limit $q_L = q_R = 1$, the Eqs. (C1), (C2) give

$$a = \frac{g_D^4 (1 - r^2)^{3/2}}{4\pi m_\Psi^2 (r^2 - 2)^2} \\ b \approx 0. \quad (\text{C5})$$

Those equations match the ones in Refs. [2, 33].

Appendix D: Higgs Decays

1. Higgs decay into dark fermions

If $m_{\Psi_i} < m_{h_1}/2 = 64.5 \text{ GeV}$, the Higgs h_1 decays into DM particles $\Psi_i = \Psi_1, \Psi_1^2$ through the s-channel with the Z' boson with a decay width given by

$$\Gamma(h_1 \rightarrow \bar{\Psi}_i \Psi_i) = \frac{m_{h_1} |y_i|^2 \sin^2(\theta)}{16\pi} \left(1 - \frac{4}{r_i} \right)^{\frac{3}{2}} \quad (\text{D1})$$

where $r_i = m_{h_1}^2/m_{\Psi_i^2}$ and

$$y_1 = y_c \\ y_2 = (Z_R)^{11} [(Z_L)^{11} (y_x)^{11} + (Z_L)^{12} (y_x)^{12}] + (Z_R)^{12} [(Z_L)^{11} (y_x)^{12} + (Z_L)^{12} (y_x)^{22}] / \sqrt{2}. \quad (\text{D2})$$

Appendix E: Z decay into dark fermions

If $m_{\Psi_k} < m_Z/2$ the decay of Z boson into dark fermions is kinematically allowed, the decay width is:

$$\Gamma(Z \rightarrow \bar{\Psi}_k \Psi_k) = \frac{g_1^2 \epsilon^2 s_W^2}{24\pi} \sqrt{1 - \frac{4}{r}} \left[(a_k^2 + b_k^2) \left(1 - \frac{1}{r}\right) + 6a_k b_k \frac{1}{r} \right], \quad (\text{E1})$$

where $a_k = (q_{\psi_L^k} - q_{\psi_R^k})$, $b_k = (q_{\psi_L^k} + q_{\psi_R^k})$, s_W is the sine of the Weinberg angle, and $r = m_Z^2/m_{\Psi_k}^2$.

Appendix F: Contribution to the number of relativistic degrees of freedom in the early Universe

Models where neutrinos are Dirac fermions can have additional contributions to the number of relativistic degrees of freedom in the early Universe [17]. Right-handed neutrinos can be in thermal equilibrium with SM plasma for non-zero kinetic mixing. To maintain equilibrium, the following condition holds:

$$\Gamma_{\nu_R}(T) > 3H n_{\nu_R}, \quad (\text{F1})$$

where H is the Hubble rate, n_{ν_R} is the number density of right-handed neutrinos and Γ is the interaction rate between right-handed neutrinos and SM plasma, which is given by:

$$\Gamma_{\nu_R}(T) = \frac{49\pi^5 T^5}{97200\zeta(3)} \left(\frac{1}{M_{Z'}}\right)^4 (g_Z^{\nu_R})^2 \sum_f N_f^C [(g_Z^{fL})^2 + (g_Z^{fR})^2], \quad (\text{F2})$$

where:

$$g_Z^{\nu_R} = 9(g_D s_{W'} + g_1 \epsilon c_{W'} s_W), \quad (\text{F3})$$

that can be approximated as $g_Z^{\nu_R} \approx 9g_1 \epsilon \sin(\theta_W)$ and g_Z^{fL} and g_Z^{fR} are the couplings of the SM fermions to the Z boson. The contribution to the ΔN_{eff} is:

$$\Delta N_{\text{eff}} = N_{\text{eff}} - N_{\text{eff}}^{\text{SM}} = N_{\nu_R} \left(\frac{T_{\nu_R}}{T_{\nu_L}}\right)^4 = N_{\nu_R} \left(\frac{g(T_{\text{dec}}^{\nu_L})}{g(T_{\text{dec}}^{\nu_R})}\right)^{4/3}. \quad (\text{F4})$$

where $T_{\text{dec}}^{\nu_R}$ is the temperature of the decoupling of the right-handed neutrinos from SM plasma and T_{ν_L} is the temperature of decoupling of left-handed neutrinos from thermal

plasma $T_{\nu_L} \sim 2.3 \text{ MeV}$.

- [1] Maxim Pospelov, Adam Ritz, and Mikhail B. Voloshin, “Secluded WIMP Dark Matter,” *Phys. Lett. B* **662**, 53–61 (2008), [arXiv:0711.4866 \[hep-ph\]](#)
- [2] Ernest Ma, “Linkage of Dirac Neutrinos to Dark U(1) Gauge Symmetry,” *Phys. Lett. B* **817**, 136290 (2021), [arXiv:2101.12138 \[hep-ph\]](#)
- [3] Diego Restrepo and David Suarez, “Effective Dirac Neutrino Mass Operator in the Standard Model With a Local Abelian Extension,” *Front. in Phys.* **10**, 838531 (2022), [arXiv:2112.09524 \[hep-ph\]](#)
- [4] K. S. Babu and Gerhart Seidl, “Simple model for (3+2) neutrino oscillations,” *Phys. Lett. B* **591**, 127–136 (2004), [arXiv:hep-ph/0312285](#)
- [5] Puneet Batra, Bogdan A. Dobrescu, and David Spivak, “Anomaly-free sets of fermions,” *J. Math. Phys.* **47**, 082301 (2006), [arXiv:hep-ph/0510181](#)
- [6] André de Gouvêa and Daniel Hernández, “New Chiral Fermions, a New Gauge Interaction, Dirac Neutrinos, and Dark Matter,” *JHEP* **10**, 046 (2015), [arXiv:1507.00916 \[hep-ph\]](#)
- [7] Davi B. Costa, Bogdan A. Dobrescu, and Patrick J. Fox, “General Solution to the U(1) Anomaly Equations,” *Phys. Rev. Lett.* **123**, 151601 (2019), [arXiv:1905.13729 \[hep-th\]](#)
- [8] Davi B. Costa, Bogdan A. Dobrescu, and Patrick J. Fox, “Chiral Abelian gauge theories with few fermions,” *Phys. Rev. D* **101**, 095032 (2020), [arXiv:2001.11991 \[hep-ph\]](#)
- [9] Nicole F. Bell, Yi Cai, and Rebecca K. Leane, “Impact of mass generation for spin-1 mediator simplified models,” *JCAP* **01**, 039 (2017), [arXiv:1610.03063 \[hep-ph\]](#)
- [10] Bob Holdom, “Two U(1)’s and Epsilon Charge Shifts,” *Phys. Lett. B* **166**, 196–198 (1986)
- [11] Leon M. G. de la Vega, R. Ferro-Hernandez, A. García-Viltres, Eduardo Peinado, and E. Vázquez-Jáuregui, “Closing the dark photon window to thermal dark matter,” (11 2023), [arXiv:2311.17987 \[hep-ph\]](#)
- [12] Chi-Fong Wong, “Anomaly-free chiral $U(1)_D$ and its scotogenic implication,” *Phys. Dark Univ.* **32**, 100818 (2021), [arXiv:2008.08573 \[hep-ph\]](#)
- [13] Nicolás Bernal, Julián Calle, and Diego Restrepo, “Anomaly-free Abelian gauge symmetries with Dirac scotogenic models,” *Phys. Rev. D* **103**, 095032 (2021), [arXiv:2102.06211 \[hep-ph\]](#)

- [14] G. Mention, M. Fechner, Th. Lasserre, Th. A. Mueller, D. Lhuillier, M. Cribier, and A. Letourneau, “The Reactor Antineutrino Anomaly,” *Phys. Rev. D* **83**, 073006 (2011), [arXiv:1101.2755 \[hep-ex\]](#)
- [15] Hooman Davoudiasl, Ryuichiro Kitano, Graham D. Kribs, and Hitoshi Murayama, “Models of neutrino mass with a low cutoff scale,” *Phys. Rev. D* **71**, 113004 (2005), [arXiv:hep-ph/0502176](#)
- [16] Julian Heeck and He Zhang, “Exotic Charges, Multicomponent Dark Matter and Light Sterile Neutrinos,” *JHEP* **05**, 164 (2013), [arXiv:1211.0538 \[hep-ph\]](#)
- [17] Julian Calle, Diego Restrepo, and Óscar Zapata, “Dirac neutrino mass generation from a Majorana messenger,” *Phys. Rev. D* **101**, 035004 (2020), [arXiv:1909.09574 \[hep-ph\]](#)
- [18] P. F. de Salas, D. V. Forero, C. A. Ternes, M. Tortola, and J. W. F. Valle, “Status of neutrino oscillations 2018: 3σ hint for normal mass ordering and improved CP sensitivity,” *Phys. Lett. B* **782**, 633–640 (2018), [arXiv:1708.01186 \[hep-ph\]](#)
- [19] Martin Bauer, Patrick Foldenauer, and Joerg Jaeckel, “Hunting All the Hidden Photons,” *JHEP* **07**, 094 (2018), [arXiv:1803.05466 \[hep-ph\]](#)
- [20] G. Bélanger, F. Boudjema, A. Pukhov, and A. Semenov, “micrOMEGAs4.1: two dark matter candidates,” *Comput. Phys. Commun.* **192**, 322–329 (2015), [arXiv:1407.6129 \[hep-ph\]](#)
- [21] G. Alguero, G. Belanger, F. Boudjema, S. Chakraborti, A. Goudelis, S. Kraml, A. Mjallal, and A. Pukhov, “micrOMEGAs 6.0: N-component dark matter,” *Comput. Phys. Commun.* **299**, 109133 (2024), [arXiv:2312.14894 \[hep-ph\]](#)
- [22] N. Aghanim *et al.* (Planck), “Planck 2018 results. VI. Cosmological parameters,” *Astron. Astrophys.* **641**, A6 (2020), [Erratum: *Astron. Astrophys.* 652, C4 (2021)], [arXiv:1807.06209 \[astro-ph.CO\]](#)
- [23] Steen Hannestad and Jes Madsen, “Neutrino decoupling in the early universe,” *Phys. Rev. D* **52**, 1764–1769 (1995), [arXiv:astro-ph/9506015](#)
- [24] M. Kawasaki, Kazunori Kohri, and Naoshi Sugiyama, “MeV scale reheating temperature and thermalization of neutrino background,” *Phys. Rev. D* **62**, 023506 (2000), [arXiv:astro-ph/0002127](#)
- [25] Rupert Coy, Jean Kimus, and Michel H. G. Tytgat, “Light from darkness: history of a hot dark sector,” (5 2024), [arXiv:2405.10792 \[hep-ph\]](#)

- [26] Mu-Chun Chen, Michael Ratz, and Andreas Trautner, “Nonthermal cosmic neutrino background,” *Phys. Rev. D* **92**, 123006 (2015), [arXiv:1509.00481 \[hep-ph\]](#)
- [27] Edward W. Kolb and Michael S. Turner, “The Early Universe,” *Front. Phys.* **69**, 1–547 (1990)
- [28] Mark Srednicki, Richard Watkins, and Keith A. Olive, “Calculations of Relic Densities in the Early Universe,” *Nucl. Phys.* **B310**, 693 (1988), [,247(1988)]
- [29] Thomas Hahn, “Generating Feynman diagrams and amplitudes with FeynArts 3,” *Comput. Phys. Commun.* **140**, 418–431 (2001), [arXiv:hep-ph/0012260](#)
- [30] R. Mertig, M. Bohm, and Ansgar Denner, “FEYN CALC: Computer algebraic calculation of Feynman amplitudes,” *Comput. Phys. Commun.* **64**, 345–359 (1991)
- [31] Vladyslav Shtabovenko, Rolf Mertig, and Frederik Orellana, “New Developments in FeynCalc 9.0,” *Comput. Phys. Commun.* **207**, 432–444 (2016), [arXiv:1601.01167 \[hep-ph\]](#)
- [32] Vladyslav Shtabovenko, Rolf Mertig, and Frederik Orellana, “FeynCalc 9.3: New features and improvements,” *Comput. Phys. Commun.* **256**, 107478 (2020), [arXiv:2001.04407 \[hep-ph\]](#)
- [33] Ernest Ma, “Connecting dark gauge symmetry to the standard model,” *Phys. Lett. B* **833**, 137282 (2022), [2203.12034 \[hep-ph\]](#)
- [34] Alexandre Alves, Asher Berlin, Stefano Profumo, and Farinaldo S. Queiroz, “Dark Matter Complementarity and the Z' Portal,” *Phys. Rev. D* **92**, 083004 (2015), [arXiv:1501.03490 \[hep-ph\]](#)
- [35] Alexandre Alves, Asher Berlin, Stefano Profumo, and Farinaldo S. Queiroz, “Dirac-fermionic dark matter in $U(1)_X$ models,” *JHEP* **10**, 076 (2015), [arXiv:1506.06767 \[hep-ph\]](#)
- [36] F. Staub, “SARAH,” (6 2008), [arXiv:0806.0538 \[hep-ph\]](#)
- [37] Florian Staub, “From Superpotential to Model Files for FeynArts and CalcHep/CompHep,” *Comput. Phys. Commun.* **181**, 1077–1086 (2010), [arXiv:0909.2863 \[hep-ph\]](#)
- [38] Florian Staub, “Automatic Calculation of supersymmetric Renormalization Group Equations and Self Energies,” *Comput. Phys. Commun.* **182**, 808–833 (2011), [arXiv:1002.0840 \[hep-ph\]](#)
- [39] Florian Staub, “SARAH 3.2: Dirac Gauginos, UFO output, and more,” *Comput. Phys. Commun.* **184**, 1792–1809 (2013), [arXiv:1207.0906 \[hep-ph\]](#)
- [40] Florian Staub, “SARAH 4 : A tool for (not only SUSY) model builders,” *Comput. Phys. Commun.* **185**, 1773–1790 (2014), [arXiv:1309.7223 \[hep-ph\]](#)

- [41] Werner Porod, “SPHeno, a program for calculating supersymmetric spectra, SUSY particle decays and SUSY particle production at e+ e- colliders,” *Comput. Phys. Commun.* **153**, 275–315 (2003), [arXiv:hep-ph/0301101](#)
- [42] W. Porod and F. Staub, “SPHeno 3.1: Extensions including flavour, CP-phases and models beyond the MSSM,” *Comput. Phys. Commun.* **183**, 2458–2469 (2012), [arXiv:1104.1573 \[hep-ph\]](#)
- [43] Adam Falkowski, Christian Gross, and Oleg Lebedev, “A second Higgs from the Higgs portal,” *JHEP* **05**, 057 (2015), [arXiv:1502.01361 \[hep-ph\]](#)
- [44] Giorgio Arcadi, Abdelhak Djouadi, and Martti Raidal, “Dark Matter through the Higgs portal,” *Phys. Rept.* **842**, 1–180 (2020), [arXiv:1903.03616 \[hep-ph\]](#)
- [45] Torben Ferber, Alexander Grohsjean, and Felix Kahlhoefer, “Dark Higgs bosons at colliders,” *Prog. Part. Nucl. Phys.* **136**, 104105 (2024), [arXiv:2305.16169 \[hep-ph\]](#)
- [46] Armen Tumasyan *et al.* (CMS), “A portrait of the Higgs boson by the CMS experiment ten years after the discovery..” *Nature* **607**, 60–68 (2022), [Erratum: *Nature* 623, (2023)], [arXiv:2207.00043 \[hep-ex\]](#)
- [47] K. S. Babu, Shreyashi Chakdar, and Vishnu P. K., “Chiral dark matter and radiative neutrino masses from gauged U(1) symmetry,” (9 2024), [arXiv:2409.09008 \[hep-ph\]](#)
- [48] Ziro Maki, Masami Nakagawa, and Shoichi Sakata, “Remarks on the unified model of elementary particles,” *Prog. Theor. Phys.* **28**, 870–880 (1962)
- [49] Michael Duerr and Pavel Fileviez Perez, “Theory for Baryon Number and Dark Matter at the LHC,” *Phys. Rev. D* **91**, 095001 (2015), [arXiv:1409.8165 \[hep-ph\]](#)
- [50] Diego Restrepo, Andrés Rivera, and Walter Tangarife, “Dirac dark matter, neutrino masses, and dark baryogenesis,” *Phys. Rev. D* **106**, 055021 (2022), [arXiv:2205.05762 \[hep-ph\]](#)
- [51] Carlos E. Yaguna and Óscar Zapata, “Singlet Dirac dark matter streamlined,” *JCAP* **06**, 049 (2024), [arXiv:2401.13101 \[hep-ph\]](#)
- [52] E. Aprile *et al.* (XENON), “First Dark Matter Search with Nuclear Recoils from the XENONnT Experiment,” *Phys. Rev. Lett.* **131**, 041003 (2023), [arXiv:2303.14729 \[hep-ex\]](#)
- [53] D. S. Akerib *et al.* (LZ), “Projected WIMP sensitivity of the LUX-ZEPLIN dark matter experiment,” *Phys. Rev. D* **101**, 052002 (2020), [arXiv:1802.06039 \[astro-ph.IM\]](#)

- [54] J. Aalbers *et al.* (DARWIN), “DARWIN: towards the ultimate dark matter detector,” *JCAP* **11**, 017 (2016), [arXiv:1606.07001 \[astro-ph.IM\]](#)
- [55] P. Cushman *et al.*, “Working Group Report: WIMP Dark Matter Direct Detection,” in *Snowmass 2013: Snowmass on the Mississippi* (2013) [arXiv:1310.8327 \[hep-ex\]](#)
- [56] J. Billard, L. Strigari, and E. Figueroa-Feliciano, “Implication of neutrino backgrounds on the reach of next generation dark matter direct detection experiments,” *Phys. Rev. D* **89**, 023524 (2014), [arXiv:1307.5458 \[hep-ph\]](#)
- [57] E. Aprile *et al.* (XENON), “Constraining the spin-dependent WIMP-nucleon cross sections with XENON1T,” *Phys. Rev. Lett.* **122**, 141301 (2019), [arXiv:1902.03234 \[astro-ph.CO\]](#)
- [58] Jeremy Mardon, Yasunori Nomura, Daniel Stolarski, and Jesse Thaler, “Dark Matter Signals from Cascade Annihilations,” *JCAP* **05**, 016 (2009), [arXiv:0901.2926 \[hep-ph\]](#)
- [59] Clarissa Siqueira, Guilherme N. Fortes, Aion Viana, and Farinaldo S. Queiroz, “Indirect Searches for Secluded Dark Matter,” *PoS ICRC2021*, 577 (2021), [arXiv:2107.04053 \[hep-ph\]](#)
- [60] M. Ackermann *et al.* (Fermi-LAT), “Searching for Dark Matter Annihilation from Milky Way Dwarf Spheroidal Galaxies with Six Years of Fermi Large Area Telescope Data,” *Phys. Rev. Lett.* **115**, 231301 (2015), [arXiv:1503.02641 \[astro-ph.HE\]](#)
- [61] H. Abdallah *et al.* (H.E.S.S.), “Search for dark matter annihilations towards the inner Galactic halo from 10 years of observations with H.E.S.S.,” *Phys. Rev. Lett.* **117**, 111301 (2016), [arXiv:1607.08142 \[astro-ph.HE\]](#)
- [62] A. Acharyya *et al.* (CTA), “Sensitivity of the Cherenkov Telescope Array to a dark matter signal from the Galactic centre,” *JCAP* **01**, 057 (2021), [arXiv:2007.16129 \[astro-ph.HE\]](#)
- [63] H. Schoorlemmer (SWG0), “A next-generation ground-based wide field-of-view gamma-ray observatory in the southern hemisphere,” *PoS ICRC2019*, 785 (2020), [arXiv:1908.08858 \[astro-ph.HE\]](#)
- [64] S. Navas *et al.* (Particle Data Group Collaboration), “Review of particle physics,” *Phys. Rev. D* **110**, 030001 (Aug 2024), <https://link.aps.org/doi/10.1103/PhysRevD.110.030001>